DIAGNOSTIC ULTRASOUND MEGAHERTZ SIGNAL DETECTION WITH MULTI-BOUNCE LASER MICROPHONE

by
Qianqian Wan

A thesis submitted to Johns Hopkins University in conformity with the requirements for

the degree of Master of Engineering

Baltimore, Maryland
August 2020

Abstract

Diagnostic ultrasound is one of the most common imaging modalities in the medical imaging field. One critical component of this imaging technology is designing sensitive receivers for detecting megahertz ultrasound signals. Currently, piezoelectric transducers have been the most widely used detectors for ultrasound signal. However, newer imaging techniques, such as photoacoustic imaging, require broader detection bandwidth and more sensitive detectors in order to work with significantly weaker signal. Conventional piezoelectric transducers may be limited in their ability to detect the full frequency bandwidth with high sensitivity, due to restricted transducer size and material composition. Sensitive and broadband ultrasound signal detecting techniques are needed for the development of advanced ultrasound imaging.

The multi-bounce laser microphone utilizes optical methods to detect the displacement of a gold-covered thin film diaphragm caused by the ultrasound signal pressure waves. This sensitive all-optical sensing technique would provide new opportunities for advanced ultrasound imaging as it is expected to achieve a higher signal-to-noise ratio (SNR) in a broader spectrum when compared with conventional transducers. Each laser beam bounce interrogating on the diaphragm would take a different optical path-length that reflects the displacement and be involved in accumulation of the ultimate phase difference between the reference and signal beams for the detector to recognize. The system was previously developed for detecting

acoustic signatures generated by explosives below 10 kHz. To demonstrate its feasibility in biomedical imaging, experimental design in this work has applied this technique to detect ultrasound signals ranging from 100kHz to 1MHz.

The results of the experiments conducted in this work prove that the multi-bounce laser microphone system is capable of detecting megahertz range ultrasound signal. As compared to the conventional fibre-optic hydrophone, the laser microphone system achieves a higher SNR as the number of bounces increases. In the test of detecting 500kHz ultrasound signal, the SNR provided by the fibre-optic hydrophone is 38dB while the one achieved by the13-bounce laser microphone is 54dB. This is a promising sensitivity enhancement with a number of potential applications for detecting signals of significantly lower power, that would otherwise be very difficult for conventional piezoelectric ultrasound transducers to detect.

Primary Reader and Advisor: Emad M. Boctor

Secondary Reader: Peter Louis Gehlbach, Ernest Marshall Graham

Acknowledgments

I am very grateful to my advisor, Professor Emad Boctor, for introducing me to the advanced techniques of photoacoustic and ultrasound imaging, and for his guidance along the road of my master research. He was always very patient for questions and gives me the chance to conduct research through trial and error.

I am also very grateful to Dr. ChenChia Wang from Brimrose Corp. for being so supportive of my research. We have worked together during many of the experiments. Dr. Wang has always generously shared his experience with me and I have learned a great deal from him on optics and the laser microphone.

I would like to express my sincere gratitude to Prof. Peter Gehlbach, and Prof. Ernest Graham for being in my master thesis reader committee. I also want to thank Prof. Raymond Koehler, Prof. Jin Kang, Dr. Jeeun Kang, Dr. Sudhir Trivedi (from Brimrose Corp.) and my fellows Keshuai, Yixuan and Hyunwoo for their great support during periods requiring trouble shooting and problem-solving in my research.

Contents

List of Tables

List of Figures

1 Introduction

For clinical diagnosis and surgical monitoring and guidance, many imaging modalities are able to non-invasively show regional anatomy and position details, but few of them are able to provide functional information. Monitoring the concentration of metabolism-related species or bio-markers could also be helpful during surgery and in interventional imaging. In retinal imaging, for example, Ophthalmoscope and Optical Coherence Tomography (OCT) allows ophthalmologists to identify micron-scale anatomical features for diagnosis and surgical guidance. Some general physiological indices that correlate with health and diseases can also be accessed through biochemical analysis. However, to determine whether the tissue in a specific anatomic location is injured, dead or healthy, more detailed physiological information is required. This may include but not be limited to metrics of blood circulation such as blood flow, oxygen saturation (sO_2), carbon dioxide (pCO_2) and other in vivo indices. Photoacoustic imaging represents a potential solution for this specific demand and has garnered research interests in the areas of structural and functional imaging. Currently, challenges to application of photoacoustic imaging fall broadly into two area: 1) the sensitivity of detection provided by the transducers and 2) safety concerns and clinical flow interruption due to laser hazards.

Piezoelectric transducers have been the most widely used ultrasound detectors. In prior work, piezoelectric transducers were also applied to detect photoacoustic signals. However, this advanced technology requires a broad detection bandwidth and highly sensitive detector in order to work with significantly weaker signals as compared to medical ultrasound imaging. Given the intrinsic characteristics of restricted transducer size and material composition, conventional piezoelectric transducers might encounter problems of limited frequency bandwidth and sensitivity of detection in applications of

photoacoustic imaging. Sensitive and broadband ultrasound and photoacoustic signal detecting techniques are needed.

The multi-bounce laser microphone is an all-optical sensing technique previously developed for detecting acoustic signatures generated by explosives below 10 kHz [2]. It is also easier to build up a compact assembly of the sensing components. This system may act as a useful detecting tool to face the challenges in applications of photoacoustic imaging as it is expected to achieve a higher signal-to-noise ratio (SNR) in a broader spectrum as compared to conventional transducers. In order to demonstrate its feasibility in detecting megahertz range ultrasound signals, we began to work on experiments since summer 2019 till now.

In this work, we will introduce the mechanism of multi-bounce laser microphone, carry out experiments with this system and compare its performance with other conventional detection methods for ultrasound signals. The experimental design is described in chapter 3. This technique has been applied to detect ultrasound signals ranging from 100kHz to 1MHz which are emitted from the single element ultrasound transducer. Results are presented in chapter 4. Chapter 5 and 6 are discussion and conclusion part of this work.

Qianqian is the research master student who set up the system in the lab, produced different phantoms, carried out the experiments following instruction from Dr. ChenChia Wang (except some of the multi-bounce tests done by Dr. ChenChia Wang at Brimrose Lab during the pandemic of COVID-19) and performed data analysis in this work. Dr. ChenChia Wang and Dr. Jeeun Kang also helped with the experimental design and setting up the laser microphone system. Mr. Keshuai Xu provided the first-generation phantoms and assisted with some of the 3D-printing tasks.

2 Background

The laser microphone is an all-optical sensing method developed for detection of pressure waves with enhanced sensitivity. The system is composed of a pulsed laser source, a beam splitter, optical lens, mirrors, and a detector based on photo-induced electromotive force (Photo-EMF) effect [3]. This approach has been previously applied in several low-frequency (<10kHz) detection scenarios such as stand-off chemical detection [2] and monitoring human life signs (e.g. heart beat and respirations) [5]. There is a research question and interest to extend this technology and evaluate detection sensitivity for diagnostic ultrasound megahertz signal range. If proved to have an enhanced sensitivity over conventional transducers, we hypothesize that this technology will address unmet needs for safe and cost-effective photoacoustic imaging and future patch ultrasound technologies.

Photoacoustic imaging provides optical contrast information of different tissue targets and absorbers combined with ultrasonic anatomy information. This technique detects acoustic waves generated by optical absorption from either endogenous light-absorbing substances like oxygenated (HbO2) and deoxygenated hemoglobin (HbR), or exogenous contrast agents such as nanoparticles and organic dyes [6]. Table 2.1 compares OCT and photoacoustic imaging technologies.

TABLE 2.1 COMPARISON BETWEEN OPTICAL COHERENCE TOMOGRAPHY AND PHOTOACOUSTIC IMAGING

Comparison/Modality	Optical Coherence Tomography	Photoacoustic Imaging
Optical Absorption Measurement	Indirect	Direct
Received Signal	Optical	Acoustic
Numerical Model	Lambert-Beer's Law	$P = \Gamma \times \mu_a \times F$ *
Imaging Depth	3mm	7cm
Minimum Resolution	3 μm	5 μm

* Γ is the Gruneisen coefficient; μ_a is the absorption coefficient; and F is the local optical fluence.

During retinal imaging, OCT technology is based on receiving optical signals reflected back from the biologic target's various optically reflective interfaces, revealing characteristic images that describe retinal anatomy in single micron scale. The optical absorption is estimated by inverse calculation based on Lambert-Beer's Law. Different from the indirect estimation conducted in OCT technology, the photoacoustic signal received is generated directly by the illumination, which indicates the optical absorption capability of the different substances in the target tissue. For the received signal, acoustic waves for photoacoustic imaging are much less scattered in tissue than the photons from the OCT modality. The useful signal penetrable depth for OCT technology is limited to few millimeters while spectroscopic photoacoustic imaging, i.e. covering multiple wavelength typically from 700-900nm, can show details at depths of up to few centimeters. It is reported that the minimum lateral resolution for retinal imaging with OCT is 3 μm, while 5 μm is achieved by optical resolution photoacoustic microscopy [6].

When applying photoacoustic imaging approaches to retinal imaging, brain imaging or other clinical fields, the main challenges fall into two areas: 1) the sensitivity of detection provided by the detectors and

2) the safety concerns regarding laser use. Either the configuration of the photoacoustic imaging system and the laser source specifications should manage to meet the criteria for safe laser exposure in biological tissue. Given the fact that maximum ocular exposure should be limited to below 100nJ/cm^2 [10], the laser illumination power may need to be significantly lower for generating acoustic signal detectable with piezoelectric transducers. Conventional piezoelectric transducers have compromised space for sensitivity enhancement due to limited sensing area size for the element and the material's intrinsic features. However, with sensitive optical sensing methods like the laser microphone, the expectation of detecting weak signal generated by illumination from lower power laser source might be satisfied.

3 Methods

3.1 Experimental set up and devices

The experimental set up design shown in Figure 3.1.1 is expanded from the design of Dr. Sudhir Trivedi and Dr. Chen-Chia Wang's previous work on enhanced sensitivity vibrometer [3]. Figure 3.1.2 shows the actual set up in the lab. A pulsed laser source is used to build up the multi-bounce laser microphone. The laser beam splits equally into reference and signal beams. The reference beam goes directly to the photo-induced-electromotive force (photo-EMF) detector (Brimrose Corp., Baltimore, MD). Pressure waves from the single element piezoelectric transducer propagate through the phantom to a gold-coated diaphragm (thickness:125μm). The diaphragm functions as a mirror where the signal beam interrogates on the propagating pressure waves before reaching the detector. Another gold mirror is placed in front of the diaphragm to realize multiple bounces. The photo-EMF detector decodes the phase difference between reference and signal beams by producing electrical currents. When detecting the pressure waves, the phase difference caused by the displacement of the diaphragm surface would be accumulated through multiple bounces of the laser signal beam, leading to a larger response expressed in output currents that enhances the sensitivity of detection.

Before using the single element piezoelectric transducer, the laser microphone system needs to pass the coherence verification step. A speaker driven by arbitrary function generator vibrates a piece of gold mirror in the optical path of the reference beam for phase modulation. Phase difference by displacement of the gold mirror surface would produce maximum output peak-to-peak difference once the optical pathlengths of the reference beam and signal beam are balanced, which verifies that the coherence between the two laser beams has been optimized.

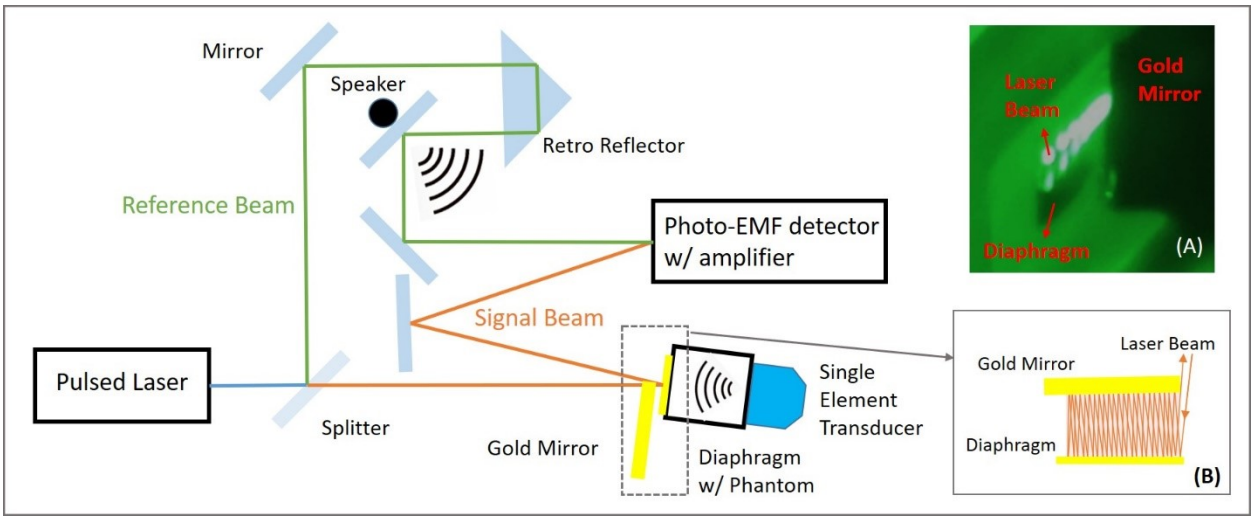

Figure 3.1.1 Design of the multi-bounce laser microphone experiment. (A). Multiple bounces of the laser beam indicated by bright spots on the gold-covered diaphragm viewed through an infrared viewer; (B). Multiple bounces between gold mirror and gold-coated diaphragm.

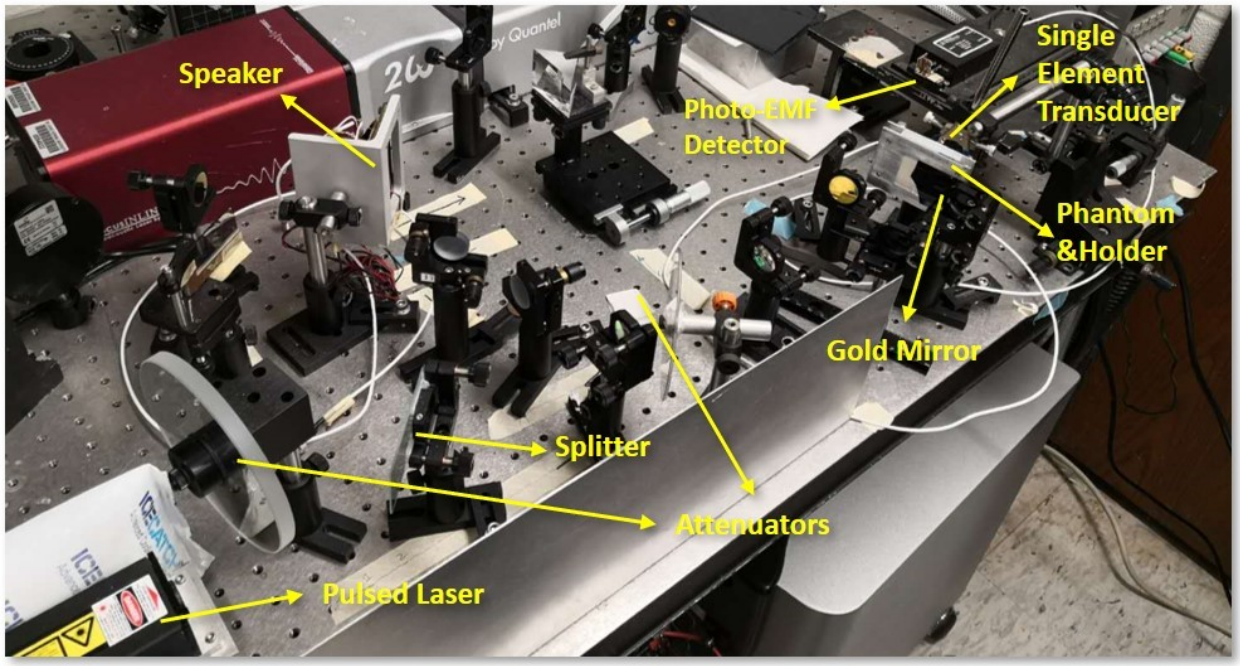

Figure 3.1.2 Experimental set up in lab

The pulsed laser source we used is the Diode Pumped Ultra-compact Q-switched IR Laser (CrystaLaser LC, Reno, NV). It emits 1064nm pulsed laser at pulse repetition rate (PRR) of 95-100kHz in the experiment. The signal beam carries information about phase modulations imposed on the thin-film diaphragm. The reference beam and signal beam interfere inside a photo-EMF detector and produce photocurrent corresponding to the temporal phase differential between the two beams. Then the photocurrent is amplified by a transimpedance amplifier (312B-1-AC/312A-4-1PF, Analog Modules Inc., Longwood, FL) and the output signal is detected and displayed on a 300 MHz oscilloscope (Digital Oscilloscope TDS 3034C, Tektronix Inc., Beaverton, OR) for data collection and interpretation.

The ultrasound single element transducers, model V318-SU and V314-SU (Olympus Scientific Solutions Americas Inc., Waltham, MA), with center frequency at 500 kHz and 1MHz respectively are used as the source of ultrasound waves. The emitted ultrasound wave propagates through the phantom before reaching the un-coated surface of the thin-film diaphragm. To drive the single element transducers, driven signal would be generated by arbitrary function generator and amplified by radio frequency power amplifier (RFA, ENI 2400).

3.2 Phantoms

The first-generation cube phantom tested was made of agar and water. It was highly transmissive to acoustic waves with an estimated attenuation coefficient of 0.0022 dB/(cm*MHz) (coefficient of water). It is shown in Figure 3.2.1 (A). The phantom has the cross-sectional area of 39.5mm * 39mm and the thickness of 44 mm. There is a 1mm-thick, 10mm-high protruding small stage at the front of the phantom to hold diaphragm from slipping away due to the gravity. A water droplet or small amount of acoustic gel would be smeared on the phantom surface above the stage to help adhere diaphragm with surface tension.

The second-generation phantom shown in Figure 3.2.2 was composed of plastic material with a cross-sectional area of 50mm*40mm and the thickness of 20mm. The attenuation coefficient of this phantom material is higher than water. We also machined an aluminum holder to improve the stability of diaphragm and phantom assembly. The L-shape holder has a 30mm*30mm opening window on one arm to expose the diaphragm and a hole for post to fixate it on the optical table.

The third-generation phantom was made of high-performance cured liquid silicone compounds Dragon Skin 10 Medium (Smooth-on Inc., Macungie, PA), which is called soft silicone from here forward. The silicone material is mixed with curing agent at a 1:1 volume. The mix is stirred well and poured into molds. The silicone compounds would cure in the 3D-printed Polylactic Acid (PLA) molds. Another material used for the third-generation phantom is high-impact urethane rubber Simpact 85A (Smooth-on Inc., Macungie, PA), which would be referred as hard silicone. The phantom making process consists of similar steps but for this material with greater hardness, the curing agent and material are mixed at 0.85:1 by weight.

In addition to varying the phantom material composition, we also evaluated different thin-film diaphragms. The uncoated thin films shown in Figure 3.2.1 (B) and (C) are made of polycarbonate and glass material. The gold-coated thin film shown in Figure 3.2.1 (D) is silica-based. After filling the silicone compounds in the mold, place a piece of thin film on the top surface before the compounds cure. After the compounds curing, the thin films would bind to the silicone phantom tightly and those uncoated thin films will have gold directly deposited on the polished surface. This is intended to improve the system repeatability by holding the thin films in place and eliminating the impact of reapplying the diaphragms between tests.

Figure 3.2.2 shows an example build-up of the ultrasound signal propagation. The single element ultrasound transducer is attached to the back of the phantom cube and the gold diaphragm attached to the center front surface of the phantom. Ultrasound signal transmitted by the single element would penetrate

through the acoustic coupling gel, the phantom, and finally reach the diaphragm. Acoustic gel acts as a acoustic coupling agent between phantom and transducer to assist with maximal acoustic pressure wave transmission.

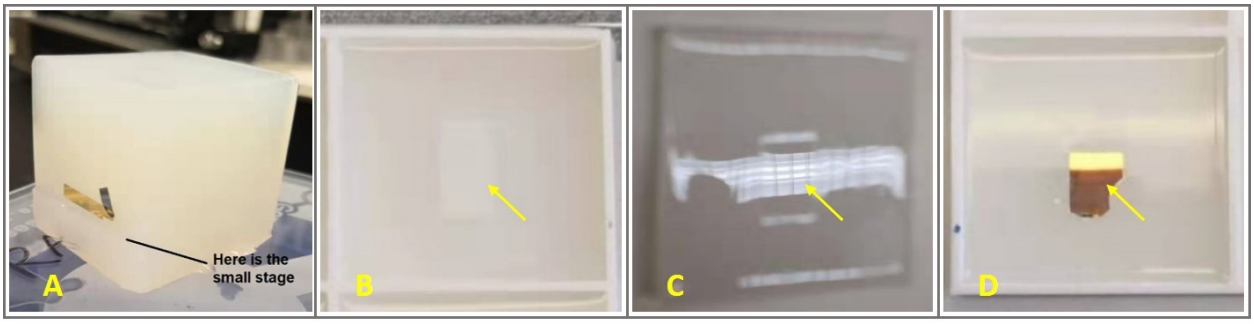

Figure 3.2.1 Different kinds of phantoms: (A) Agar phantom; Silicone phantoms with (B) polished polycarbonate thin films (C) glass thin film; (D) gold-coated silica-based diaphragm.

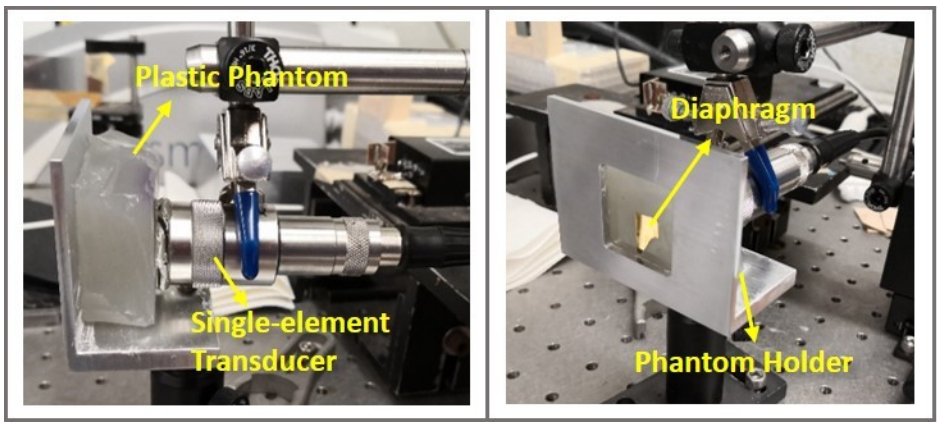

Figure 3.2.2 Mounting of diaphragm, plastic phantom, L-shape aluminum phantom holder and single element piezoelectric transducer

A 3D-printed phantom holder is designed to alternate the aluminum holder and improve the stability of the mounting and repeatability of the system. Figure 3.2.3(A) shows one assembly of ① 3D-printed holder, ② silicone phantom and ③ gold-deposited polycarbonate diaphragm. In Figure 3.2.3 (B), ① is the cap

and ② is the base of the holder. To make an assembled phantom, combine the two parts together with protruding features facing inwards and fill it with silicone compounds. The small protruding features would act as 'stops' to help prevent the phantom from exhibiting any rotational motion after the silicone compounds cured. The holder is about 50mm in diameter and 10mm in thickness.

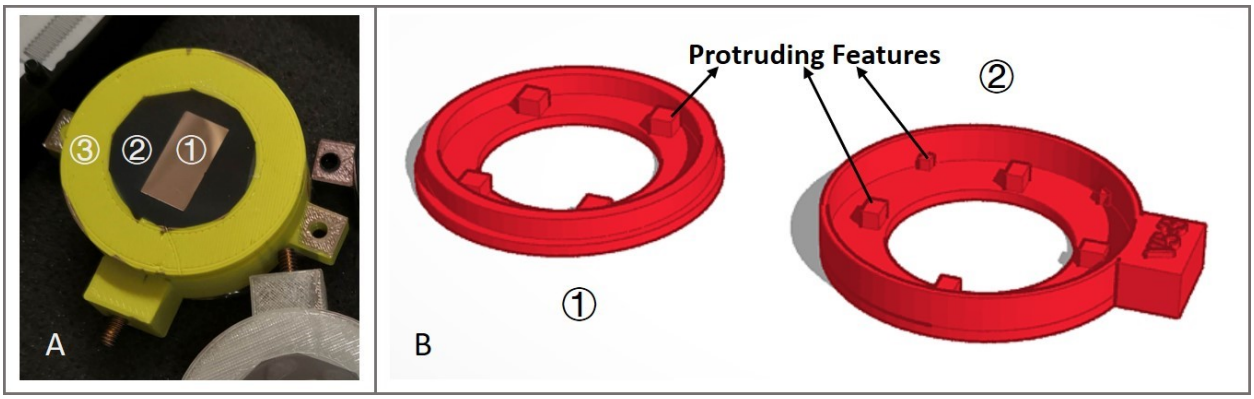

Figure 3.2.3 Pictures of 3D-printed phantom holder. (A) Assembled phantom; (B) 3D design of the phantom holder

Most recent phantom holder design trials are printing out 2 sets of phantom holders and fill them with hard and soft silicone product respectively. In each set of holders, there are several different holder designs (see Table 3.1). The parabolic holder design shown in Figure 3.2.4 has its inner surface follow the paraboloid $y = \frac{1}{16} * x^2$. The focal point is at the height of 4mm. Cut the paraboloid shape at 4mm height and the polycarbonate thin film would be placed at this cut plane after pouring in silicone compounds and before it cures.

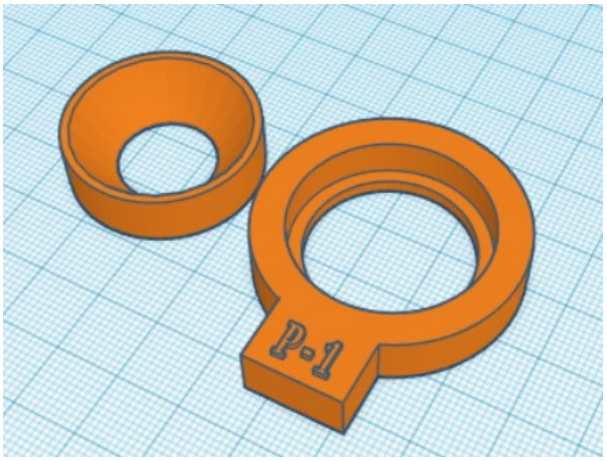

Figure 3.2.4 Parabolic Holder Design

TABLE 3.1 NEW PHANTOM HOLDER DESIGN TRIALS

Number	Thickness (mm)	Diameter (mm)	Front/Back Opening (Diameter in mm)	Size of Polycarbonate Film / Special Design
1	10	40	26 / 26	10mm*20mm
2	10	40	16 / 26	10mm*10mm
3	5	40	16 / 26	10mm*10mm
4	10.25	40	16 / 26	10mm*10mm / Parabolic Inner Surface
5	5	40	16 / 26	None
6	5	40	37.6 / 26	None

3.3 Optical hydrophone test

The purpose of this test is to know what the signal should look like after penetrating the phantom and compare it with the one detected by laser microphone. The optical hydrophone (Fibre-optic Hydrophone System, Precision Acoustics Ltd., Dorset, UK) is applied to detect ultrasound signal emitted from single

element ultrasound transducer using the similar set up for laser microphone test. Figure 3.3.1 shows an example of set up for the optical hydrophone test. The fiber end of the optical hydrophone points vertically to the phantom's front surface, detecting the ultrasound signal emitted by the single element ultrasound transducer and horizontally propagated through the phantom.

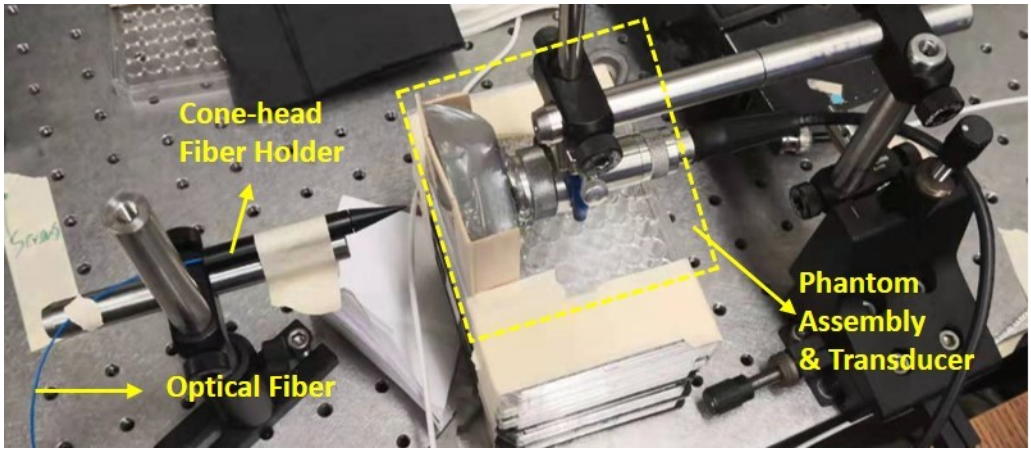

Figure 3.3.1 Set-up of optical hydrophone test

3.4 Data collection and analysis process

When detecting continuous signal, the oscilloscope is triggered by the sync output of the arbitrary function generator for driven signal. For pulsed mode signal, the oscilloscope is triggered by the pulsed mode control signal. The raw data of low frequency signal (<=100kHz, i.e. the speaker output) is collected under peak detect acquisition mode of the oscilloscope. For higher frequency signal, the raw data is collected under envelop acquisition mode (frame number: 512) to take multiple frames overtime and display all collected data points in single frame, which helps to overcome the problem caused by pulsed laser's limited PRR. Export the data in '.csv' format.

The raw data of continuous wave detection was processed with envelop detection and frequency analysis in MATLAB. The oscilloscope exports each dataset with 10000 data points. The data processing steps are:

1) Import the selected file of raw data, plot the signal in time domain. An example is shown in Figure 3.4.1 (A).
2) Perform envelope detection for the traces as results shown in Figure 3.4.1 (B).
3) Perform fast fourier transform (FFT) process.
4) Plot the absolute FFT value and also provide a semilogy plot. Examples are presented in Figure 3.4.1 (C) and (D).
5) Calculate the SNR of detected signal based on absolute FFT value plot.

The SNR is determined by the formula:

$$SNR = 20 * \log_{10}(\frac{A_{signal}}{A_{noise}})\ dB.$$

A_{signal} is the peak absolute FFT value, while A_{noise} is the absolute FFT value at around 10 times higher frequency of the signal center frequency (peak frequency).

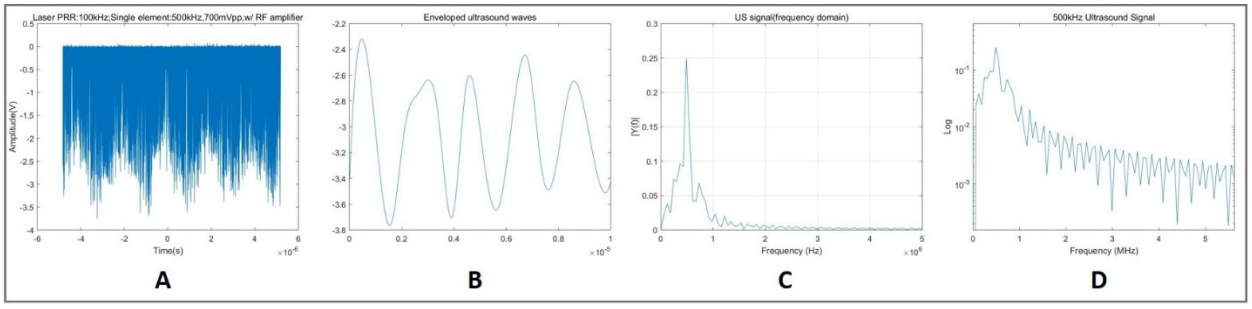

Figure 3.4.1 Data analysis process

4 Results

4.1 Coherence verification

We check the coherence of the two laser beams by driving a speaker behind one of the mirrors in the reference beam path-length with kHz range sinewave signal and observing the output from the oscilloscope. The signal we detected from the speaker is about 2Vpp in amplitude sitting on top of the laser pulses and it is shown in Figure 4.1.1. The speaker is driven by sinusoid signal of 2kHz, 800mVpp and 1Vdc from function generator. The laser PRR is 100kHz level as marked in the title of the figures. The actual PRR we used in the experiments is 96-99kHz. It would be a little different each time we switch the laser on, so usually the laser would be free running till the end of experiments once it is on.

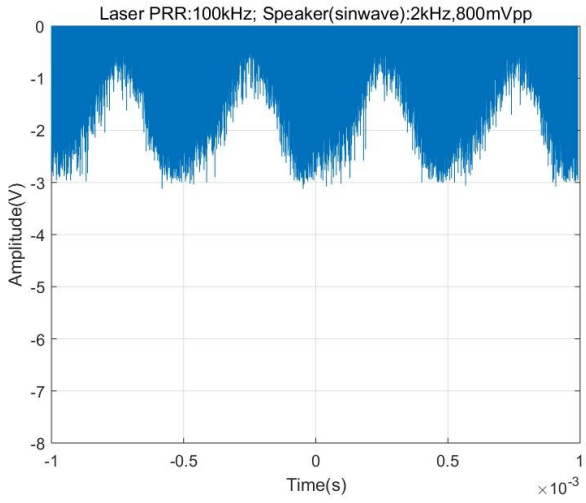

Figure 4.1.1 Coherence verification

4.2 Continuous ultrasound signal detection

Except for the experiments of detecting 1MHz continuous wave ultrasound signals, all the other experiments have applied the single element ultrasound transducer V318-SU (Olympus Scientific Solutions Americas Inc., Waltham, MA).

4.2.1 Agar phantom

The single element transducer is driven by signal generated from arbitrary function generator and amplified by the RFA. Figure 4.2.1.1 and Figure 4.2.1.2 are the 500kHz continuous sinewave ultrasound signal detection of laser microphone and optical hydrophone respectively. The laser microphone can achieve near 1.5Vpp output amplitude for detected signal and the optical hydrophone achieves 20mVpp output amplitude.

Laser microphone SNR_{agar}= 40dB.

Optical hydrophone SNR_{agar}= 51dB.

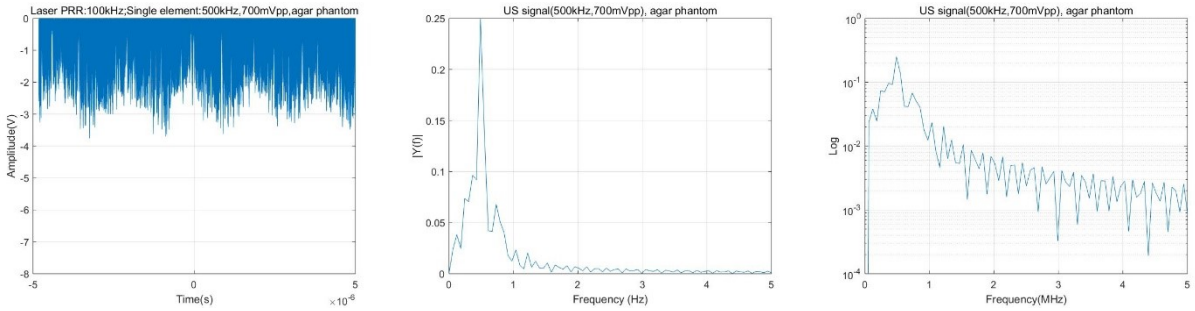

Figure 4.2.1.1 Laser microphone detection of 500kHz continuous wave signals with agar phantom

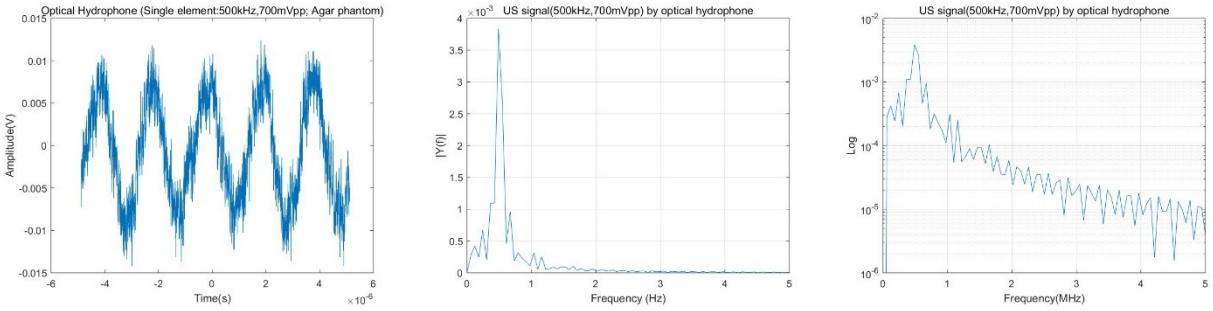

Figure 4.2.1.2 Optical hydrophone detection of 500kHz continuous wave signals with agar phantom

According to the manual, the single element transducer V318-SU reaches half-maximum intensity output when operated with signal input of 310kHz and 710kHz. Figure 4.2.1.3 show the detected signals from single element transducer V318-SU driven by 310kHz (left) and 710kHz (right) sine wave signals. Comparing to results in Figure 4.2.1.2, the laser microphone can achieve about 0.8Vpp output, approximately half of the output amplitude the system could achieve when single element transducer was driven at its center frequency of 500kHz.

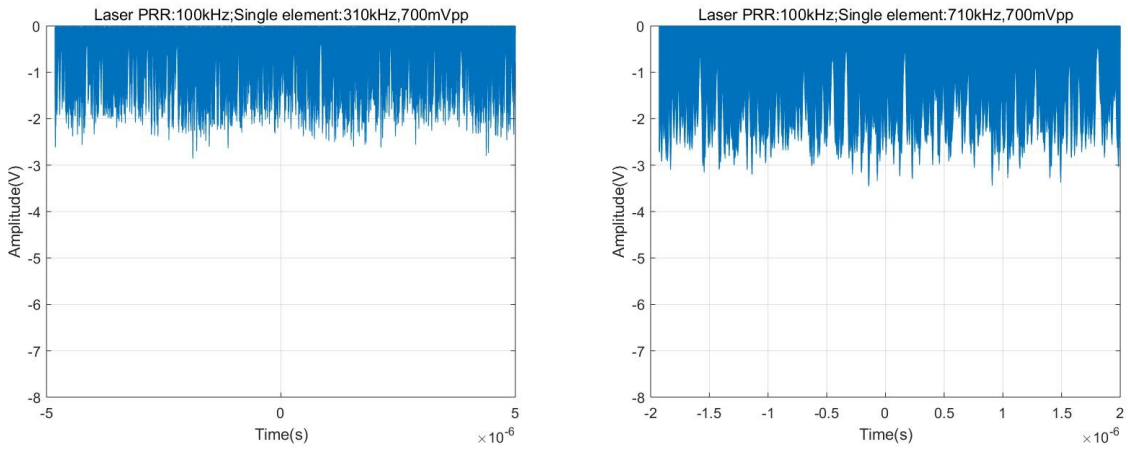

Figure 4.2.1.3 Laser microphone detection of continuous wave signals of different frequency with single element transducer V318-SU

Figure 4.2.1.4 present the detection 1MHz ultrasound signal emitted from single element transducer V314-SU (center frequency at 1MHz). The laser microphone can achieve about 1Vpp output amplitude. This proves that the system is capable of detecting megahertz range ultrasound signals.

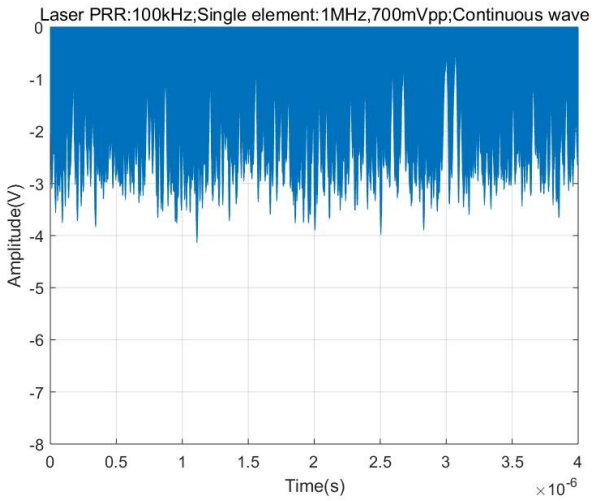

Figure 4.2.1.4 Laser microphone detection of 1MHz continuous wave signals with single element transducer V314-SU

4.2.2 Plastic phantom

Figure 4.2.2.1 and Figure 4.2.2.2 show the continuous ultrasound wave detection of laser microphone and optical hydrophone respectively. The laser microphone can achieve near 2Vpp output for detected signal and the optical hydrophone achieves 50mVpp for the detected signal.

Laser microphone $SNR_{plastic}$= 38 dB.

Optical hydrophone $SNR_{plastic}$= 37 dB.

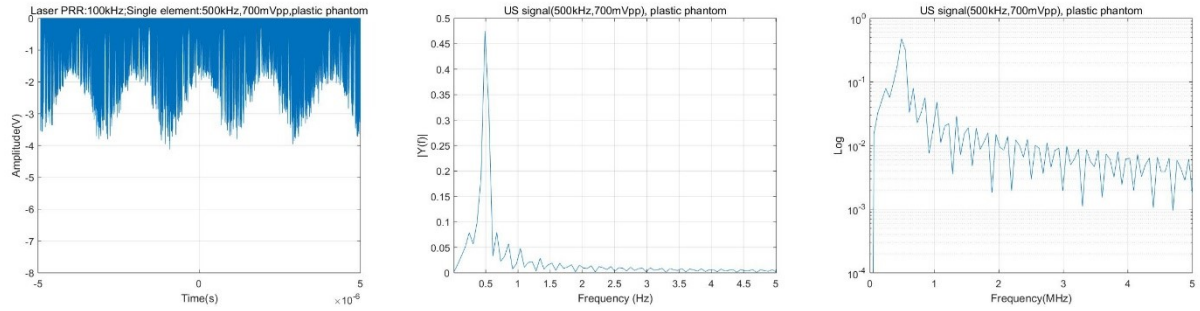

Figure 4.2.2.1 Laser microphone detection of 500kHz continuous wave signals with plastic phantom

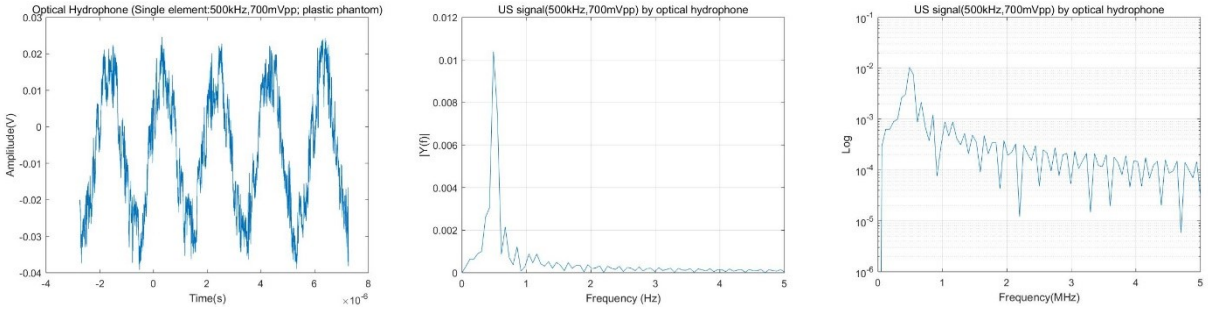

Figure 4.2.2.2 Optical hydrophone detection of 500kHz continuous wave signals with plastic phantom

4.2.3 Silicone phantom

Figure 4.2.3.1 and Figure 4.2.3.2 show the continuous ultrasound wave detection of laser microphone (only one bounce) and optical hydrophone respectively. The laser microphone can achieve near 1Vpp output for detected signal and the optical hydrophone achieves 30mVpp for the detected signal.

Laser microphone $SNR_{silicone}$(485kHz) = 30dB.

Optical hydrophone $SNR_{silicone}$(500kHz) = 38dB.

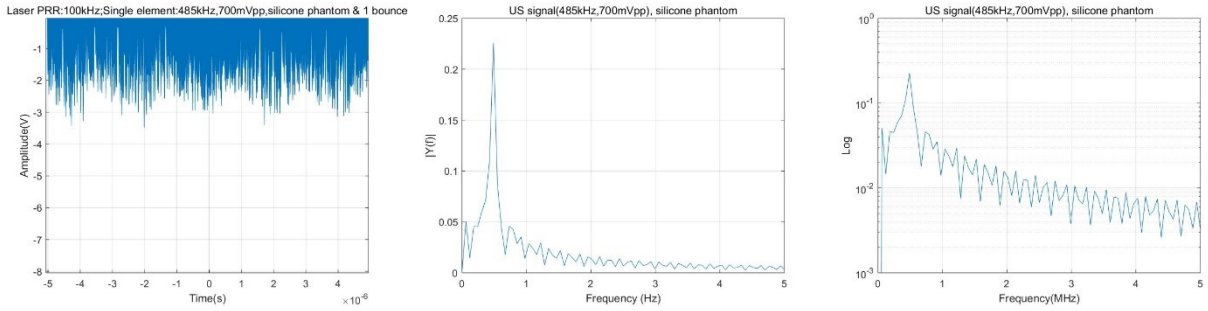

Figure 4.2.3.1 Laser microphone detection of 485kHz continuous wave signals with silicone phantom

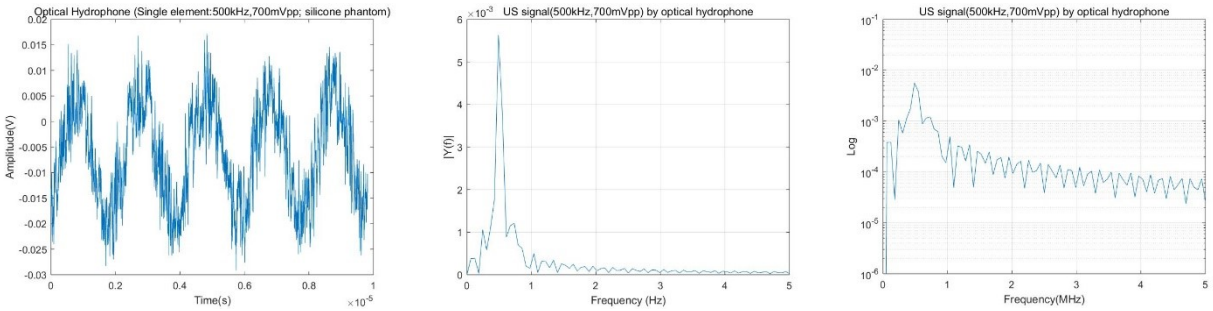

Figure 4.2.3.2 Optical hydrophone detection of 500kHz continuous wave signals with silicone phantom

Figure 4.2.3.3, Figure 4.2.3.4 and Figure 4.2.3.5 present the continuous ultrasound wave detected by multi-bounce laser microphone of 3 bounces, 13 bounces and 21 bounces respectively. The laser microphone can achieve near 1Vpp output for 3-bounce test and 1.5Vpp for 21-bounce test. Note that the experiment setup for 13-bounce and 21-bounce laser microphone is different as no RFA is included. For 13-bounce and 21-bounce setup, the driving signal applied on the single element ultrasound transducer varies from 10Vpp to 26Vpp. For 3-bounce setup, the driving signal from function generator is 700mVpp and then amplified by RFA (Gain≈50dB). It is estimated as 220Vpp driving voltage for the single element transducer, more than 10 times higher than that of 21-bounce setup. Following are the data analysis figures and calculated SNR results of the multi-bounce tests.

$SNR_{3\text{-bounce}}$ (485kHz) = 38 dB;

$SNR_{3\text{-bounce}}$ (500kHz) = 33 dB;

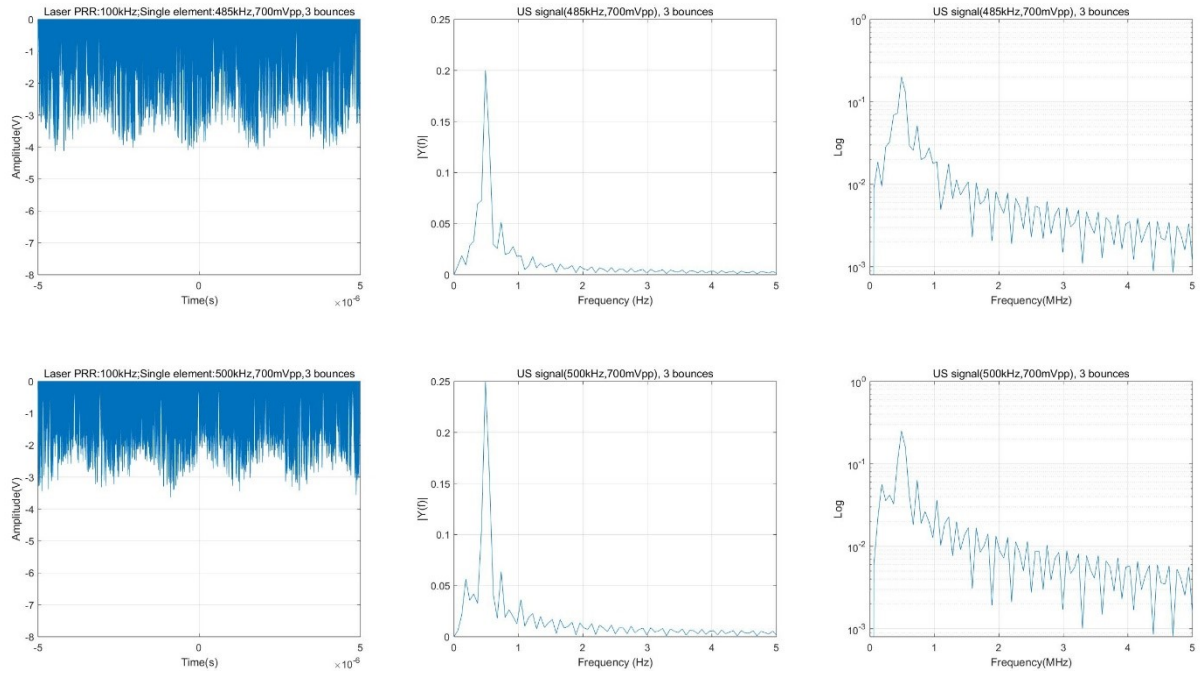

Figure 4.2.3.3 3-bounce laser microphone detection of 485kHz and 500kHz continuous wave signals with silicone phantom

(Following data are collected from experiments done by Dr. ChenChia Wang at Brimrose lab)

$SNR_{13\text{-bounce}}$ (500kHz, 20Vpp) = 43dB;

$SNR_{13\text{-bounce}}$ (500kHz, 15Vpp) = 54dB;

$SNR_{13\text{-bounce}}$ (500kHz, 10Vpp) = 44dB;

$SNR_{21\text{-bounce}}$ (500kHz, 26Vpp) = 42 dB;

$SNR_{21\text{-bounce}}$ (500kHz, 20Vpp) = 40 dB;

$SNR_{21\text{-bounce}}$ (500kHz, 15Vpp) = 41 dB;

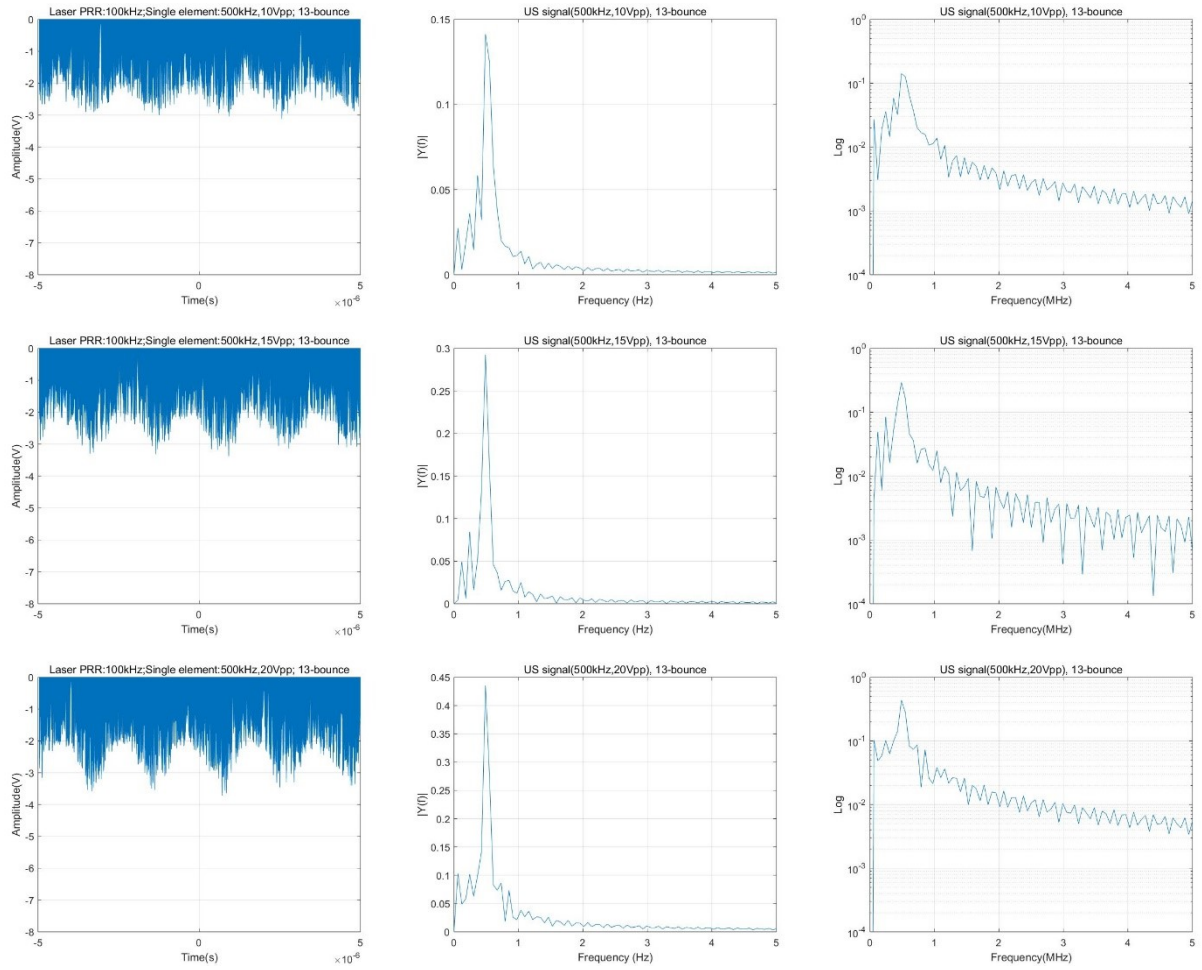

Figure 4.2.3.4 13-bounce laser microphone detection of 500kHz continuous wave signals with silicone phantom and different driving voltage for single element ultrasound transducer

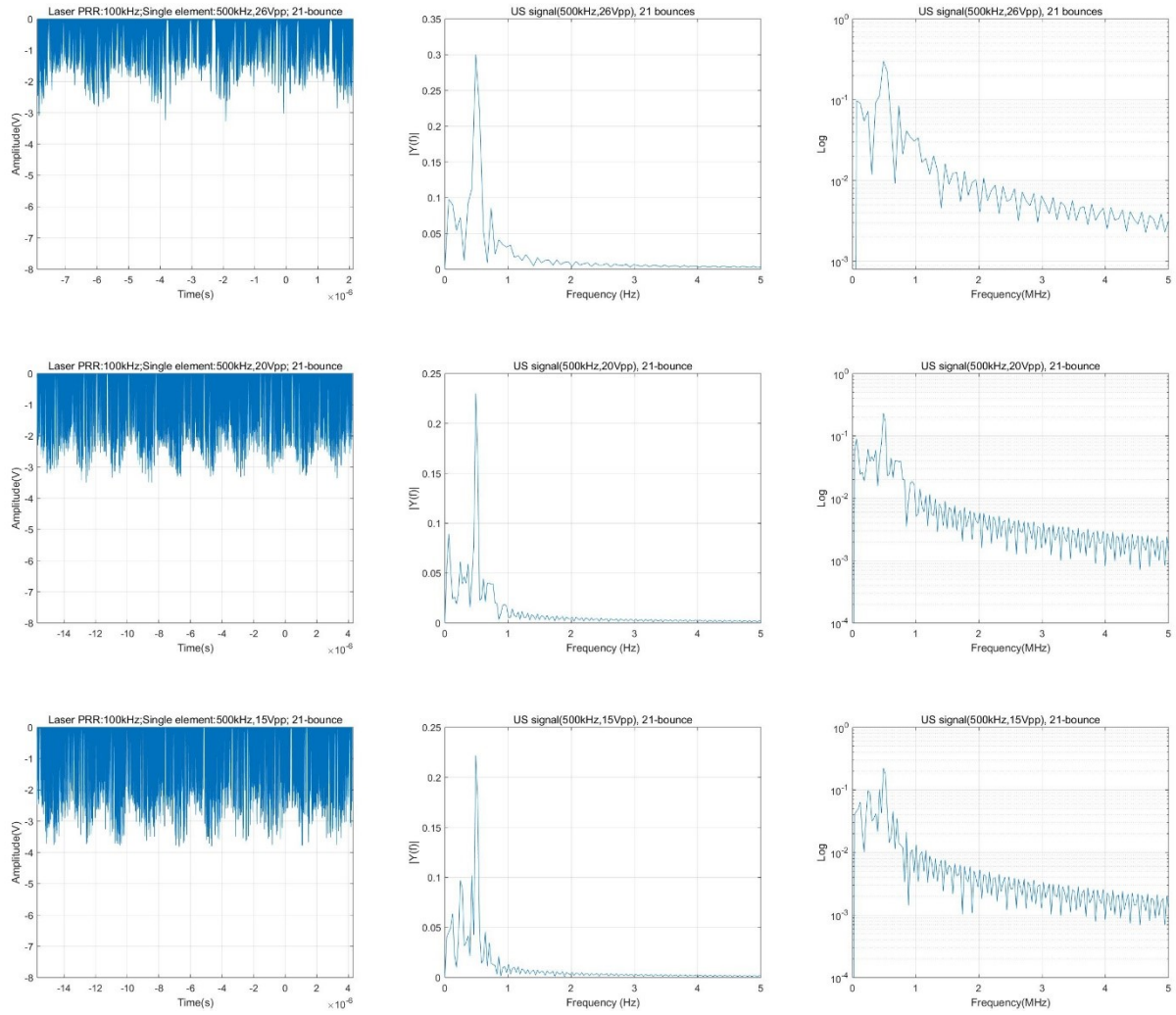

Figure 4.2.3.5 21-bounce laser microphone detection of 500kHz continuous wave signals with silicone phantom and different driving voltage for single element ultrasound transducer

4.3 Pulsed mode sine wave ultrasound signal detection

4.3.1 Agar phantom

The results below are taken from a similar experimental set up of continuous ultrasound signal detection. To realize the pulsed mode ultrasound signal excitation, we add one more arbitrary function generator to control the driving signal of single element ultrasound transducer. The 500kHz single element transducer V318-SU is driven by a pulsed mode sine wave ultrasound signal. An arbitrary function generator outputs 500kHz, 700mVpp sine wave signal to the RF amplifier. For pulsed mode, another function generator is used as a trigger input to control the on-and-off of the 500kHz sine wave cycles coming out. In this test, we set 3 sine wave cycles per 10us for 500kHz pulsed mode signal. Figure 4.3.1.1. and Figure 4.3.1.2 present detected traces in different time scale and indicate the activated cycles for pulsed mode signal in yellow rectangular boxes. In Figure 4.3.1.1, we can compare the traces of continuous wave and pulsed mode wave in the same time scale. As indicated in the figure at the right-hand side, there are at least 3 full cycles of sinewave at around 30us to 40us and each cycle is appearing at the approximately same position where the cycle within the continuous wave is located.

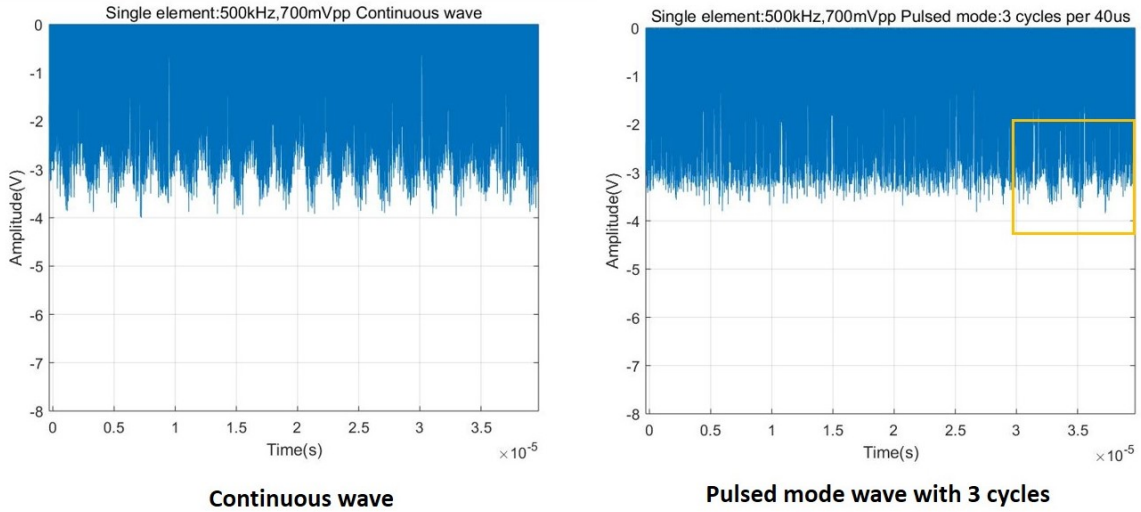

Figure 4.3.1.1 Detected continuous and pulsed mode ultrasound signals in 4us time scale

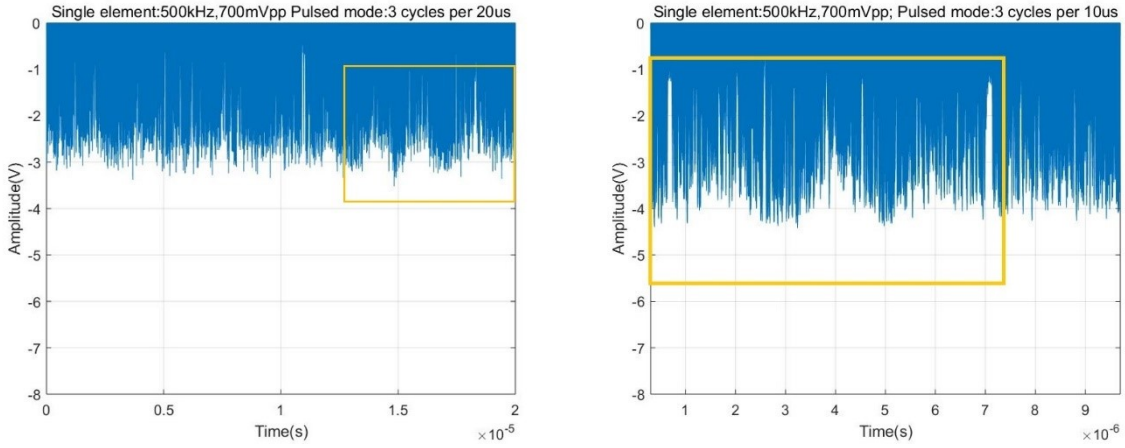

Figure 4.3.1.2 Pulsed mode ultrasound signals of different repetition rate displayed in different time scale

4.3.2 Plastic phantom

In this test, we set 2 sine wave cycles per 10us for 500kHz pulsed mode signal. The detected cycles are indicated by the yellow rectangular box in Figure 4.3.2.1.

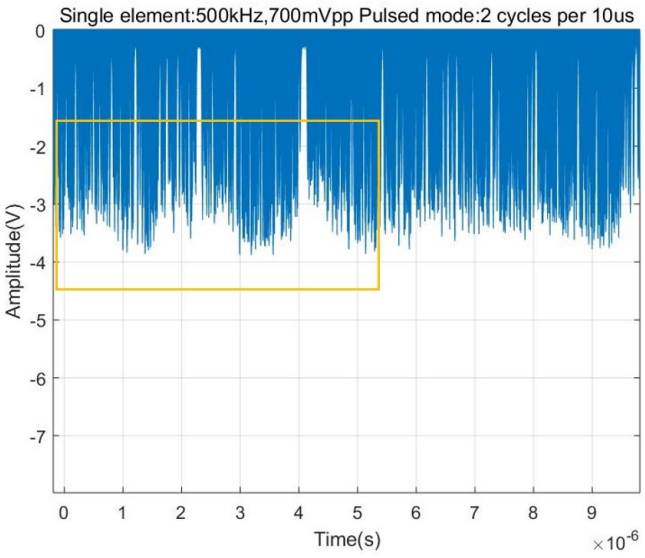

Figure 4.3.2.1 Pulsed mode ultrasound signals detection with plastic phantom

The temporal data traces and screenshot from the oscilloscope in Figure 4.3.2.2 show what the pulsed ultrasound signal waveform looks like. The signal was detected by fibre-optic hydrophone in this figure. The 2-cycle pulsed wave signals were detected every 10us with a specific fixed delay after the trigger signal's rising edge.

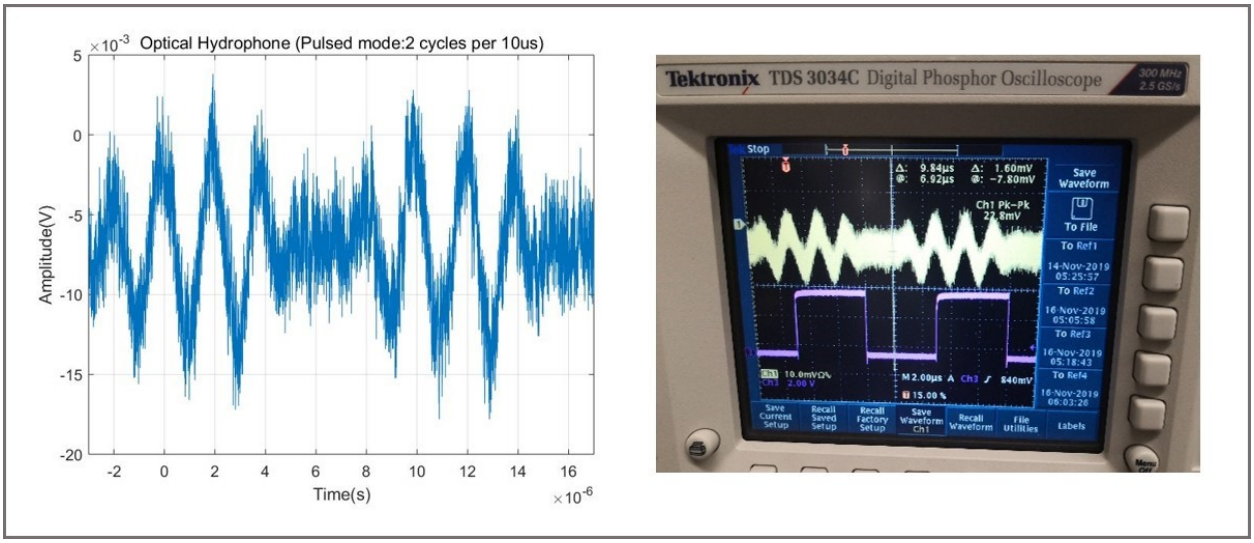

Figure 4.3.2.2 Pulsed mode ultrasound signals detected by optical hydrophone

5 Discussion

With this system, we can detect megahertz sinewave signal in both continuous wave and pulsed mode wave. However, viewing from the oscilloscope, due to the limited storage of data points and the relatively low SNR we can achieve at this point, we could only observe a few cycles on the display screen. After replacing the agar phantom with plastic phantom and silicone phantom, and reducing the distance of the acoustic signal penetration, the detected signal strength was raised up and the data collected contained less noise. To date, we have tried several new phantom designs to further improve the stability of the set up. We have also introduced 21 multiple bounces in this system set up.

5.1 Phantom performance and system stability

The agar phantom would shrink overtime due to dehydration in air. The phantom was measured to be 1mm shorter after one-hour exposure in air, as compared to the measurement done immediately after removing from water. The rate of dehydration would diminish over time.

Observations have shown that acoustic gel (or water) applied on the phantom surface would also dry up during the test. The influence of dehydration problem includes diaphragm distortion and changes in optical path-length of the signal laser beam. We had spent a lot of time adjusting the angles of optical lens to balance the optical path-lengths before collecting test data. These were the main for evaluating new phantom materials, such as plastic material and silicone compounds which are not affected by dehydration problem and much easier to preserve.

The plastic and silicone phantoms resist precision cutting therefore it was useful to develop a molding technique for phantom production. Silicone phantoms are easier to produce as compared to silicone phantoms as the process does not require heating at high temperature and high melting point molds.

To assist with holding the phantom tightly in the system and improving the repeatability, we have designed 3D-printed phantom holders. The ultimate goal of the design was to bring the thin film diaphragm and the phantom media into a compact assembly which would create uniform and stable contact with the signal source. The opening facing the single element ultrasound transducer is designed to be about the same size as the transducer so that once the holder is fixed, we are able to attach the signal source back to the exact position and repeat the test.

The new trial using silicone with a greater hardness index helps to eliminate phantom deformation due to attaching and detaching the transducer between tests. The deformation is deleterious to the function of laser microphone detection because the diaphragm (or the gold surface) can be distorted, affecting the stability of the multi-bounce part. After switching to hard silicone, the phantom is less deformable, thereby improving the test reproducibility.

5.2 Potential applications

The potential applications of the multi-bounce laser microphone are presently directed at detecting ultrasound and photoacoustic signals that are generated with much lower illumination power. In many clinical scenarios, photoacoustic imaging with high power laser is not considered safe. A LED light source system may help to maintain the laser power at a safe level and move photoacoustic imaging technology as a clinical modality forward. The higher SNR provided by this multi-bounce laser microphone system is an essential point for the detection of relatively weak acoustic signal generated by illumination using the LED system.

6 Conclusion

Experiments have proved the multi-bounce laser microphone is capable to detect megahertz range continuous wave ultrasound signals as well as some pulsed wave signals. Some of SNR results of the tests are listed in Table 6.1. For 485kHz ultrasound signals, we compare the performance of detection between one-bounce and 3-bounce system. For 500kHz ultrasound signals, we compare the performance between 3-bounce and 13-bounce system. It can be indicated that the SNR of multi-bounce laser microphone can be improved as number of bounces increases. To date, we have succeeded in introducing 21 bounces in this system, but the 21-bounce system hasn't been adjusted into the stable condition for repeatable tests. We still need to improve the quality of the gold surface on the diaphragm to enable more bounces between the gold surfaces. To achieve this goal, different gold deposition strategies and methods for making the assembled phantom need to be tested.

TABLE 6.1 TEST RESULTS OF ULTRASOUND SIGNAL WITH MULTI-BOUNCE LASER MICROPHONE AND SILICONE PHANTOM

#	Number of Bounces	Frequency	Driving Voltage for Single element	SNR (dB)
1	1	485kHz	220V	30
2	3	485kHz	220V	38
3	3	500kHz	220V	33
4	13	500kHz	10V	44
5	13	500kHz	15V	54
6	13	500kHz	20V	43

Figure 6.1 shows the comparison between signals detected with the multi-bounce laser system and the conventional optical hydrophone system. Even with much lower driving voltage for the single element ultrasound transducer, which means less powerful emitted ultrasound signal to be detected, the multi-bounce laser microphone system can still outperform conventional optical hydrophone in SNR for the detection of 500kHz ultrasound signals.

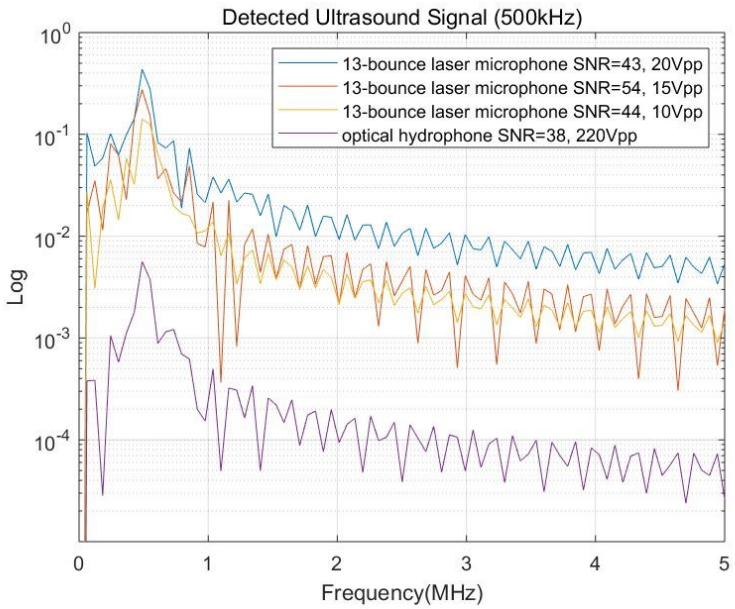

Figure 6.1 Comparison between ultrasound signal detected with different system

In the future, we are planning to increase the number of bounces to further enhance the sensitivity and do experiments on detecting ultrasound signals in a higher frequency range as well as broad-band photoacoustic signal. The technique shows its potential in several biomedical applications such as photoacoustic retinal imaging, which requires a highly sensitive detector for photoacoustic signal generated from low illumination power, which would be very difficult for conventional piezoelectric transducers to detect.

7 Bibliography

[1] Wissmeyer, Georg, et al. “Looking at Sound: Optoacoustics with All-Optical Ultrasound Detection.” Light: Science & Applications, vol. 7, no. 1, Springer Science and Business Media LLC, Aug. 2018.

[2] Gupta, Deepa, et al. “Stand-Off Chemical Detection Using Photoacoustic Sensing Techniques—From Single Element to Phase Array.” Chemosensors, vol. 6, no. 1, MDPI AG, Jan. 2018, p. 6.

[3] Trivedi, Sudhir, et al. “ENHANCED SENSITIVITY VIBROMETER.” US 8072609 B1, United States Patent, Dec. 2011.

[4] Pepper, D. M., et al. “Characterization of the Photo-Emf Response for Laser-Based Ultrasonic Sensing Under Simulated Industrial Conditions.” Review of Progress in Quantitative Nondestructive Evaluation, Springer US, 1998, pp. 627–34.

[5] Wang, Chen-Chia, et al. “Human Life Signs Detection Using High-Sensitivity Pulsed Laser Vibrometer.” IEEE Sensors Journal, vol. 7, no. 9, Institute of Electrical and Electronics Engineers (IEEE), Sept. 2007, pp. 1370–76.

[6] Li, Mucong, et al. “Photoacoustic Tomography of Blood Oxygenation: A Mini Review.” Photoacoustics, vol. 10, Elsevier BV, June 2018, pp. 65–73.

[7] Nguyen, Van, and Yannis Paulus. “Photoacoustic Ophthalmoscopy: Principle, Application, and Future Directions.” Journal of Imaging, vol. 4, no. 12, MDPI AG, Dec. 2018, p. 149.

[8] Zhang, Hao F., et al. “Photoacoustic Ophthalmoscopy for In Vivo Retinal Imaging: Current Status and Prospects.” Ophthalmic Surgery, Lasers, and Imaging, vol. 42, no. 4, SLACK, Inc., July 2011, pp. S106–15.

[9] Song, Wei, et al. “A Combined Method to Quantify the Retinal Metabolic Rate of Oxygen Using Photoacoustic Ophthalmoscopy and Optical Coherence Tomography.” Scientific Reports, vol. 4, no. 1, Springer Science and Business Media LLC, Oct. 2014.

[10] American National Standards Institute, and Laser Institute of America. American National Standard for Safe Use of Lasers. Laser Inst of America, 2014, pp. 62–85.

[11] Guggenheim, J.A., Li, J., Allen, T.J. et al. Ultrasensitive plano-concave optical microresonators for ultrasound sensing. Nature Photon 11, 2017, pp. 714–719.

8 Vita

Qianqian Wan was born in China in 1996. She received the B.S. degree in Biomedical Engineering from Zhejiang University, Hangzhou, China, in 2018. She is expected to receive the MSE degree in Biomedical Engineering from Johns Hopkins University Whiting School of Engineering in August 2020.